JACS
JOURNAL OF THE AMERICAN CHEMICAL SOCIETY
Article
pubs.acs.org/JACS

Dendrite-Free Lithium Deposition via Self-Healing Electrostatic Shield Mechanism

Fei Ding,[†,∥] Wu Xu,*[,†] Gordon L. Graff,[†] Jian Zhang,[†] Maria L. Sushko,[‡] Xilin Chen,[†] Yuyan Shao,[‡] Mark H. Engelhard,[§] Zimin Nie,[†] Jie Xiao,[†] Xingjiang Liu,[∥] Peter V. Sushko,[‡,⊥] Jun Liu,[‡] and Ji-Guang Zhang*[,†]

[†]Energy and Environment Directorate, [‡]Fundamental and Computational Sciences Directorate, and [§]Environmental and Molecular Sciences Laboratory, Pacific Northwest National Laboratory, Richland, Washington 99354, United States

[∥]National Key Laboratory of Power Sources, Tianjin Institute of Power Sources, Tianjin 300381, People's Republic of China

[⊥]University College London, London WC1E 6BT, United Kingdom

Supporting Information

ABSTRACT: Rechargeable lithium metal batteries are considered the "Holy Grail" of energy storage systems. Unfortunately, uncontrollable dendritic lithium growth inherent in these batteries (upon repeated charge/discharge cycling) has prevented their practical application over the past 40 years. We show a novel mechanism that can fundamentally alter dendrite formation. At low concentrations, selected cations (such as cesium or rubidium ions) exhibit an effective reduction potential below the standard reduction potential of lithium ions. During lithium deposition, these additive cations form a positively charged electrostatic shield around the initial growth tip of the protuberances without reduction and deposition of the additives. This forces further deposition of lithium to adjacent regions of the anode and eliminates dendrite formation in lithium metal batteries. This strategy may also prevent dendrite growth in lithium-ion batteries as well as other metal batteries and transform the surface uniformity of coatings deposited in many general electrodeposition processes.

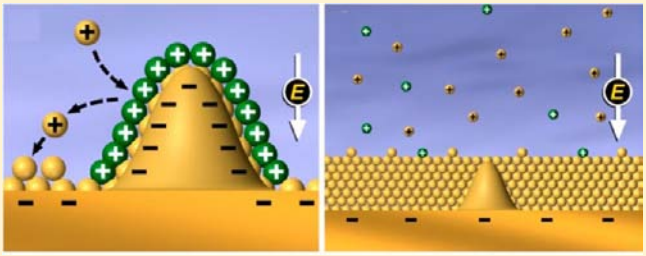

INTRODUCTION

Lithium (Li) metal has an extremely high theoretical specific capacity (3860 mAh g^{-1}), low density (0.59 g cm^{-3}), and the lowest negative electrochemical potential (−3.040 V vs standard hydrogen electrode (SHE)); thus rechargeable Li metal batteries have been called the "Holy Grail" of energy storage systems and have been investigated extensively during the last 40 years.[1−5] The Li metal anode has also been widely used in the investigation of "next generation" rechargeable batteries, such as Li-sulfur batteries[6,7] and Li-air batteries.[8,9] However, two major problems, Li dendrite growth and low Coulombic efficiency during repeated charging and discharging, hinder commercial application of Li metal-based cells.[5,6,10,11] Although the Coulombic efficiency problem can be compensated by using excess Li metal, without significantly compromising the energy density of the batteries,[2] Li dendrite growth during long-term cycling often leads to short circuits and sometimes even catastrophic failure. In the last 40 years, Li dendrite formation has been widely observed,[5,10−14] analyzed,[15−17] and simulated.[18−20] Most approaches to dendrite prevention focus on improving the stability and uniformity of the solid electrolyte interface (SEI) layer by adding SEI formation additives.[11,12,20−29] However, the additives used in these studies are consumed as part of the SEI films so they are ineffective in suppressing Li dendrite during long-term operation. As indicated by Aurbach,[11] it is very difficult to achieve sufficient passivation with Li electrodes and liquid solutions. The approach to form alloys with Li metal during deposition process has also been reported, which is achieved by adding inorganic compounds or second salts into the electrolytes.[30−33] However, due to the consumption of such metal cation additives by forming alloys during Li deposition, the suppression to Li dendrite formation is not sustainable. As an alternative, various mechanical barriers have been proposed to block dendrite growth.[18,34,35] Most of these approaches rely on a strong mechanical barrier (SEI film or separator) to suppress the Li dendrite growth but do not change the fundamental, self-amplification behavior of the dendrite growth. A general solution to the dendrite growth problem will not only enable a series of Li metal-based energy storage systems, but also benefit general electrodeposition processes widely used in industry.

We propose and demonstrate a novel mechanism, which can fundamentally alter dendrite formation in electrochemically deposited lithium films. Fundamental principles behind this mechanism will be analyzed. Various characterization and modeling tools have been used to analyze the morphology of

Received: December 22, 2012
Published: February 28, 2013

   dx.doi.org/10.1021/ja312241y | J. Am. Chem. Soc. 2013, 135, 4450−4456

the deposited lithium films and simulate their formation process. The details of these analysis and long-term test results of Li metal batteries will be reported in this work.

EXPERIMENTAL SECTION

Materials and Li Deposition. $LiPF_6$, propylene carbonate (PC), and dimethyl carbonate (DMC) were purchased from Novolyte in battery grade. KPF_6 (99.9%) was obtained from Alfa Aesar. CsI (99.999%), RbI (99.9%), and $AgPF_6$ (98%) were ordered from Sigma-Aldrich. $CsPF_6$ and $RbPF_6$ were synthesized by mixing stoichiometric amounts of $AgPF_6$ and the related iodide salt in PC solution inside a glovebox (MBraun) filled with purified argon where the oxygen and moisture content was less than 1 ppm, followed by filtration of the formed AgI from the solution using 0.45 μm syringe filters. $LiPF_6$ was then added into the $CsPF_6$–PC or $RbPF_6$–PC solutions to get the electrolytes.

Li was deposited on copper (Cu) foil substrates (10 mm × 10 mm) in different electrolyte solutions at the desired current densities inside the argon-filled glovebox using a Solartron electrochemical interface (SI 1287). After deposition, the electrode was washed with DMC to remove the residual electrolyte and dried in the antechamber of the glovebox under vacuum prior to characterization and analyses.

Characterization. The surface morphologies of the deposited lithium (Li) electrodes were measured by scanning electron microscopy (SEM) using a JEOL 5900 scanning electron microscope at a working distance of 12 mm and an accelerating voltage of 20 keV. Meanwhile, the surface element components were determined by means of energy dispersive X-ray fluorescence spectrometer (EDX) (JEOL 2010). To avoid air contamination, the Li electrode samples were transferred in the Sample-Saver Storage Container (South Bay Technology, Inc., U.S.) filled with purified argon and loaded into the SEM machine in a glovebag purged with pure argon.

The compositions of the SEI layers formed on the surfaces of deposited Li films were analyzed by X-ray photoelectron spectroscopy (XPS). XPS measurements of the Li samples were performed with a Physical Electronics Quantera scanning X-ray microprobe with a focused monochromatic Al Kα X-ray (1486.7 eV) source for excitation and a spherical section analyzer. The samples were mounted onto the standard sample holder inside a nitrogen recirculated glovebox operated at <0.2 ppm O_2 and a dew point of −80 °C.

The composition of each element in the deposited films was determined by inductively coupled plasma/atomic emission spectrometry (ICP/AES, Optima 7300DV, Perkin-Elmer) techniques after appropriate dilution. Three emission lines were chosen for each element as a cross-check for spectral interference. The calibration standards were matrix-matched in water.

Battery Performance Test. To prepare the Li electrodes for morphology study after long-term cycling with different electrolytes, Lil$Li_4Ti_5O_{12}$ coin cells of CR2032 type were used. The $Li_4Ti_5O_{12}$ electrode was prepared by coating a slurry of $Li_4Ti_5O_{12}$, Super P conductive carbon, and poly(vinylidene fluoride) (PVDF) (8:1:1 by weight) in *N*-methylpyrrolidone (NMP) onto a copper foil, evaporating the NMP solvent, and drying at about 80 °C under vacuum overnight. The cells were assembled inside the argon-filled glovebox with a $Li_4Ti_5O_{12}$ electrode, a glass fiber separator (500 μm thick, Whatman GF-B), a Li foil (0.75 mm thick), and 200 μL of electrolyte. They then were charged (Li deposition) and discharged (Li dissolution) between 2.5 and 1.0 V on an Arbin battery testing system (BT2000). After 100 cycles, Li anodes were taken out of the cells and washed with anhydrous dimethyl carbonate DMC for SEM observations.

Modeling and Simulations. To simulate Li deposition process in electrolytes with PC solvent and different salts (either $LiPF_6$ or $LiPF_6$/$CsPF_6$ mixture), a mesoscopic model was developed. In this model, ions were considered as spheres with the radii equal to the corresponding ionic radii. The positive and negative ions interact with each other via Coulomb force, excluded volume, and ion correlation interactions evaluated analytically within the classical Density Functional Theory approach.[37,38] Li ions that came in direct contact with the electrode surface were considered deposited on the electrode, and therefore changed the shape of the electrode surface. This, in turn, led to the change in the electrostatic potential from the electrode. To account for this effect, Laplace equation with the boundary conditions corresponding to the new shape of the electrode was solved. The equilibrium distribution of ions was then evaluated in the electrostatic field of the modified electrode. Simulations were repeated for 24 steps of Li deposition and performed at 298 K.

RESULTS AND DISCUSSION

Self-Healing Electrostatic Shield (SHES) Mechanism. We propose a self-healing electrostatic shield (SHES) mechanism that can fundamentally change the Li deposition morphology. It leads to a "self-healing" as opposed to "self-amplification" of the initial protuberant tips that unavoidably occur during the Li deposition process. This mechanism depends on an electrolyte additive cation that has an effective reduction potential lower than that of Li ion.

Figure 1 illustrates how the SHES mechanism can self-heal Li growth tips. During the initial stage of deposition, both Li ions

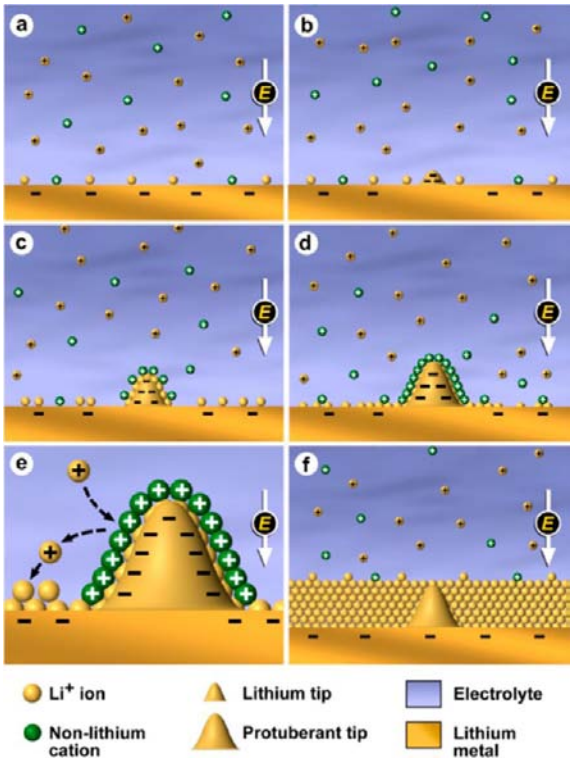

Figure 1. Illustration of Li deposition process based on the SHES mechanism.

(Li^+) and the cations of the non-Li additive (M^+) are adsorbed on the Li substrate surface (Figure 1a) under an applied voltage (V_a) slightly lower than the Li reduction potential (E_{Li/Li^+}) but higher than the additive reduction potential (E_{M/M^+}); that is, $E_{Li/Li^+} > V_a > E_{M/M^+}$, Li will be deposited on the substrate and unavoidably form some protuberant tips due to various fluctuations in the system (Figure 1b). It is well-known that a sharp edge or protrusion on the electrode exhibits a stronger electrical field, so more Li will be preferentially deposited around the tips rather than on smooth regions of the anode. In a conventional electrolyte, amplification of this behavior will form Li dendrites as reported previously.[10] However, the adsorbed additive cations (M^+) with a reduction potential lower

dx.doi.org/10.1021/ja312241y | J. Am. Chem. Soc. 2013, 135, 4450−4456

than V_a (Figure 1c) will not electroplate on the tip. Instead, they will accumulate in the vicinity of the tip to form an electrostatic shield (Figure 1d). This positively charged shield will repel incoming Li^+ from the protrusion forcing further Li^+ deposition to adjacent regions of the anode (Figure 1e) until a smooth deposition layer is formed (Figure 1f). The process repeats with formation of additional growth tips. This self-healing mechanism can effectively disrupt the conventional dendrite amplification mechanism and lead to the deposition of a smooth Li film.

The SHES mechanism depends on an additive cation (M^+) that exhibits an effective reduction potential E_{red} less than that of Li^+. According to the Nernst equation:

$$E_{Red} = E^{\phi}_{Red} - \frac{RT}{zF} \ln \frac{\alpha_{Red}}{\alpha_{Ox}} \quad (1)$$

where R is the universal gas constant (8.314472 J K^{-1} mol^{-1}), T is the absolute temperature (assume T = 298.15 K in this work), and α is the chemical activity for the relevant species (α_{Red} is for the reductant and α_{Ox} for the oxidant). $\alpha_x = \gamma_x c_x$, where γ_x and c_x are the activity coefficient and the concentration of species x. F is the Faraday constant (9.64853399 × 10^4 C mol^{-1}), and z is the number of moles of electrons transferred. Although Li^+ has the lowest standard reduction potential ($E^{\circ}_{Red}(Li^+)$) among all of the metals when measured at standard conditions [1 mol L^{-1} (M)], another cation (M^+) may have an effective reduction potential lower than that of Li^+ if M^+ has an chemical activity α_x lower than that of Li^+. In the case of low concentration, α_x can be simplified to equal the concentration c_x; then eq 1 can be simplified as:

$$E_{Red} = E^{\phi}_{Red} - \frac{0.05916V}{z} \log_{10} \frac{1}{\alpha_{Ox}} \quad (2)$$

The effective reduction potentials (vs SHE) of selected metal cations at various concentrations were calculated according to eq 2 and listed in Table 1 (assuming the activity coefficients γ_x = 1). When the concentration of cations of cesium (Cs^+) or rubidium (Rb^+) is less than 0.05 M in the electrolyte, their effective reduction potentials (see the shaded cells in Table 1) are lower than that of Li^+ at 1.0 M concentration (−3.040 V). As a result, in a mixed electrolyte where the additive (Cs^+ or Rb^+) concentration is much lower than the Li^+ concentration, these additives should not be deposited at the Li deposition potential and do not form thin layers of Li alloys at the electrode surface. In contrast, the inorganic additives (including Mg^{2+}, Al^{3+}, Zn^{2+}, Ga^{3+}, In^{3+}, and Sn^{2+}) used in the previous studies[30,31] do not have an effective reduction potential lower than that of Li^+ even though the concentrations of these additives are much lower than those of Li^+ (see Table S1 in the Supporting Information). Therefore, the proposed SHES mechanism cannot be applied to the conventional inorganic additives. Instead, as indicated by Matsuda et al.,[31] these inorganic ions form thin layers of Li alloys at the electrode surface during cathodic deposition of Li, and the resulting films suppress the dendritic deposition of Li. These additive metal ions will be consumed during each deposition, and their effectiveness will fade soon with increasing cycles.

Table 1. Effective Reduction Potentials of Two Selected Alkali Cations at Different Concentrations

	E° (V)[a]	effective reduction potential (V)			
cations	1 M	0.001 M	0.01 M	0.05 M	0.1 M
Li^+	−3.040				
Cs^+	−3.026	−3.203	−3.144	−3.103	−3.085
Rb^+	−2.980	−3.157	−3.098	−3.057	−3.039

[a]Note: E° is the standard reduction potential (vs SHE) of the cation at 1 M concentration.

In addition to a low concentration (c_x) of the additive, an activity coefficient (γ_x) of the additives lower than those of the Li^+ would also reduce the chemical activity of the cations and further lead to an effective reduction potential lower than that of Li^+. In addition, a cation that has a much lower solvation number than those of Li^+ in the given solvent will be highly efficient to form the required electrostatic shield.

Dendrite-Free Li Films Deposited with SHES Additives. The proposed SHES mechanism has been successfully verified experimentally. The effect of $CsPF_6$ concentration in the electrolyte on the prevention of Li dendrite formation and growth was then investigated. 1 M $LiPF_6$ in PC was used as the control electrolyte. The maximum concentration of $CsPF_6$ in the control electrolyte is approximately 0.055 M as determined from ICP/AES analysis; therefore, the effect of Cs^+ concentration on the final morphologies of deposited Li films was tested up to 0.05 M. SEM images of the deposited Li films on copper substrates are shown in Figure 2. Conventional Li dendritic formation is clearly observed in the Li film deposited in the control electrolyte without the $CsPF_6$ additive (Figure 2a). For the Li films deposited in electrolytes containing the Cs^+ additive, film topography decreases with increasing Cs^+ concentration. Even at very low Cs^+ concentrations (0.001 and 0.005 M), dendrite formation is substantially decreased (Figure 2b and c, respectively). Further increase in the Cs^+ concentration to 0.01 and 0.05 M results in a very distinctive improvement in anode surface quality with complete elimination of dendrite formation (Figure 2d and e). As the SHES mechanism predicts, Cs^+ cations can effectively prevent Li dendrite growth. More specifically, the Li deposition film resulting from the 0.05 M Cs^+ electrolyte becomes mirror-like to the naked eye. These results indicate that, to form an effective electrostatic shield that prevents Li dendrite growth, the additive cations not only need to have an effective reduction potential very close to that of Li^+ in the given electrolyte, but also need to have sufficiently high concentration to form the electrostatic shield. Therefore, a concentration of 0.05 M $CsPF_6$ in the control electrolyte was used in subsequent experiments. In addition to Cs^+, Rb^+ was also effective in preventing Li dendrite growth as the SHES mechanism predicts. A very fine surface morphology without dendrite formation has been observed for 0.05 M $RbPF_6$ in the electrolyte of 1 M $LiPF_6$/PC (see Figure S1 in the Supporting Information).

Further testing showed the SHES mechanism can also be used to eliminate pre-existing dendrites formed on electrodes. A highly dendritic Li film (see Figure 3a) was intentionally deposited on a copper substrate in a control electrolyte of 1 M $LiPF_6$ in PC for 1 h, then transferred into a Cs^+-containing electrolyte (0.05 M $CsPF_6$ in 1 M $LiPF_6$/PC), and deposition continued for an additional 14 h. Unlike the dendritic and mossy film deposited in the control electrolyte for the same length of time (see Figure 2a), a smooth Li film was obtained as shown in Figure 3b. The open spaces shown in Figure 3a have been filled by dense Li deposition, and all of the original needle-like dendritic whiskers have been transformed into much smaller spherical particles, which are also eliminated

dx.doi.org/10.1021/ja312241y | J. Am. Chem. Soc. 2013, 135, 4450−4456

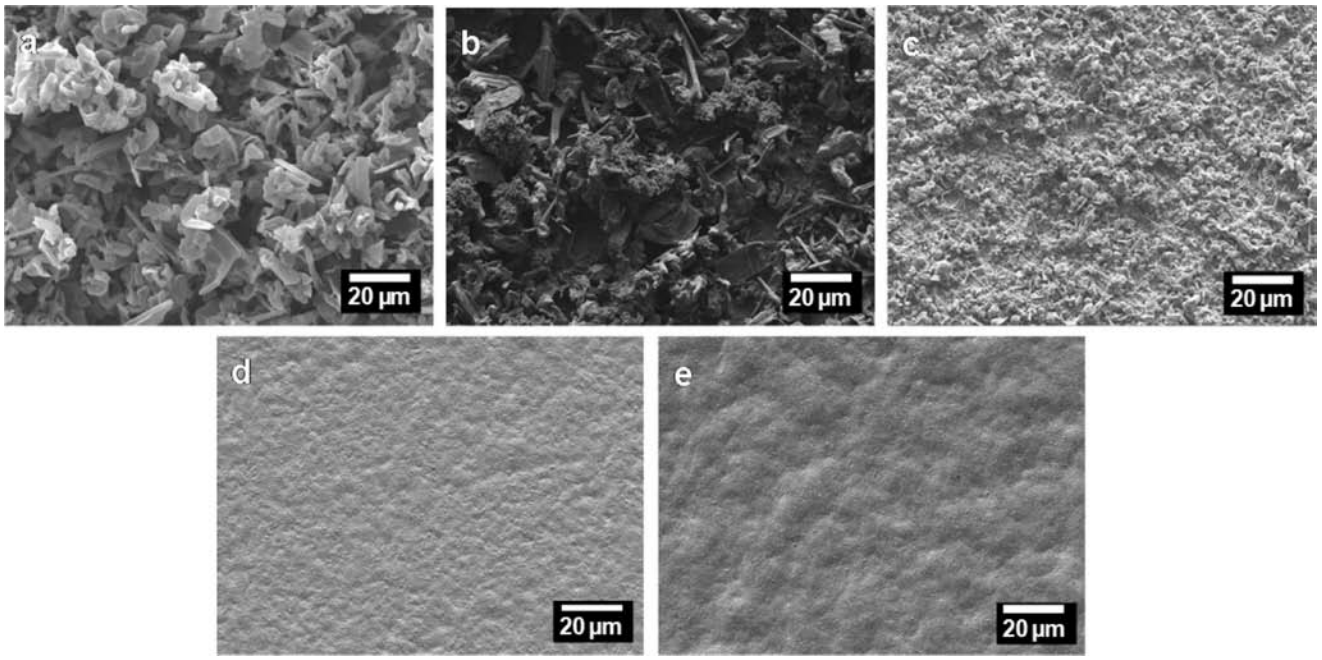

Figure 2. SEM images of the morphologies of Li films deposited in electrolyte of 1 M $LiPF_6$/PC with $CsPF_6$ concentrations of (a) 0 M, (b) 0.001 M, (c) 0.005 M, (d) 0.01 M, and (e) 0.05 M, at a current density of 0.1 mA cm^{-2}.

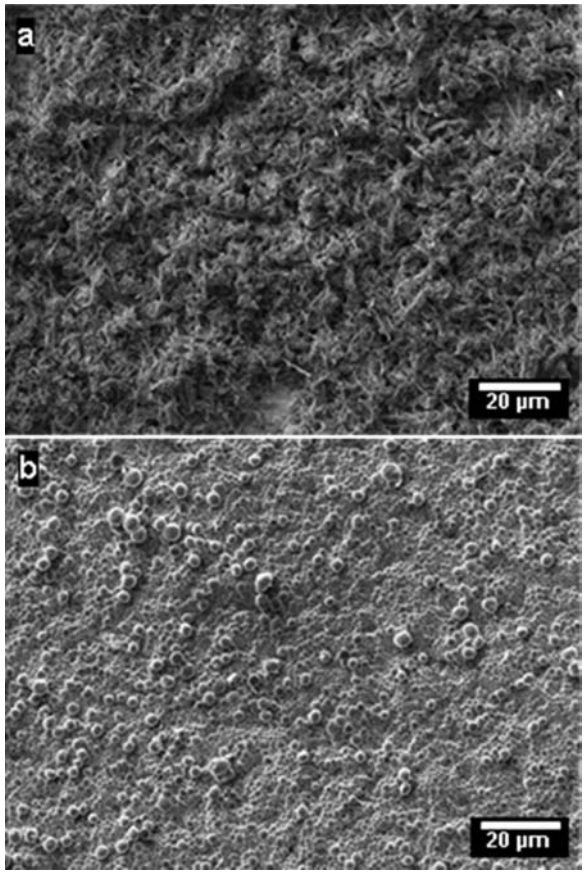

Figure 3. SEM SEM images of deposited Li films: (a) preformed dendritic Li film deposited in a control electrolyte (1 M $LiPF_6$/PC) for 1 h; (b) the same film after another 14 h Li deposition in the electrolyte with additive (0.05 M $CsPF_6$).

upon further Li deposition. We observed that all films deposited using SHES additives consisted of many small spherical particles. This is in strong contrast with the needle-like dendrites grown from a conventional electrolyte and clearly validates that the SHES mechanism has fundamentally changed the dynamic behavior of Li deposition.

In addition to the static SEM images of the deposited films, two distinguished lithium growth patterns were also directly observed and recorded by video camera attached to a microscope (see method 2.1 and Figure S4 in the Supporting Information). Movies S1 and S2 in the Supporting Information were taken during lithium deposition processes without and with 0.05 M Cs^+ additive in the control electrolyte (1 M $LiPF_6$ in PC), respectively. The deposition lasts for 5 h at a current density of 0.2 mA cm^{-2}. For the lithium film deposited without the additive, conventional dendritic growth is clearly observed. In contrast, when the lithium film was deposited in the electrolyte with 0.05 M Cs^+, the deposited lithium film exhibits a densely packed structure. These dramatic changes demonstrate that the SHES mechanism fundamentally changes the dynamics of lithium film growth from a self-amplification/disordered process to a self-healing/ordered process.

Sustainable Operation of SHES Mechanism. A critical feature of the SHES mechanism is that the adsorbed additive cations not be reduced nor incorporated into the Li surface during deposition. This feature is markedly different from previous approaches[3,28,32,33] where additives are reduced during the deposition process and "sacrificed or consumed" as part of the SEI film or an alloy to suppress Li dendrite growth.[28,31,36] As a result, the additive concentration in the electrolyte will decrease with an increasing number of charge/discharge cycles, and the effectiveness quickly degrades. In contrast, the cations used in the SHES mechanism form an electrostatic shield or "cloud" when dendritic tips initiate, which dissipates once the applied voltage is removed, thus eliminating loss of the additive upon repeated cycling. To verify this prediction, Li films (containing a SEI surface layer) deposited in electrolytes containing 0.05 M Cs^+, and 0.05 M Rb^+ additives, were analyzed by XPS, EDX, and ICP/AES . Within the instrument

dx.doi.org/10.1021/ja312241y | J. Am. Chem. Soc. 2013, 135, 4450−4456

detection limits, the test results show no evidence of Cs or Rb in the deposited Li films (including the SEI surface layers) (see Figures S2 and S3 and Table S2 in the Supporting Information for XPS, EDX, and ICP/AES analysis results, respectively).

The SHES effect was also examined in rechargeable Li metal batteries. Coin cells of the Li|$Li_4Ti_5O_{12}$ battery system were assembled using the electrolytes with and without 0.05 M Cs^+ additive. Figure 4 compares the morphologies of Li metal

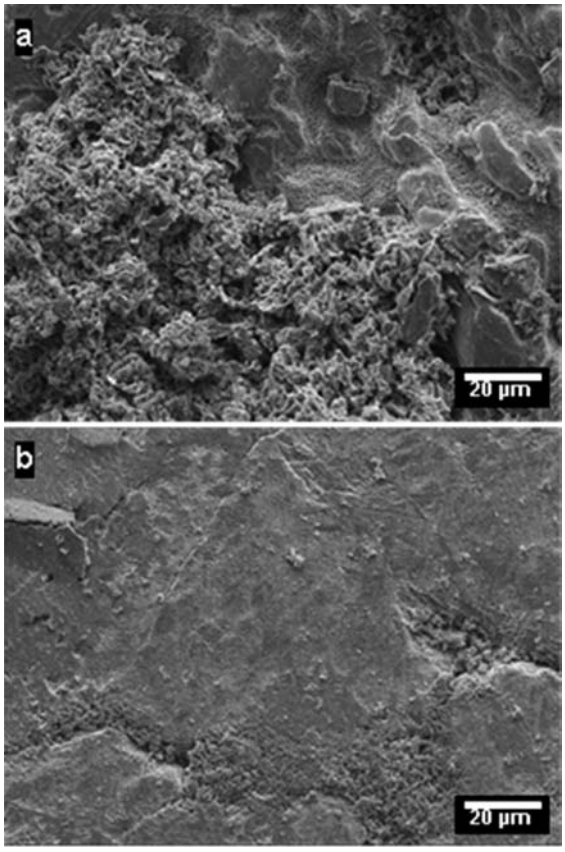

Figure 4. Morphologies of Li electrodes after 100 charge/discharge cycles in coin cells of Li|$Li_4Ti_5O_{12}$ containing electrolytes (a) without and (b) with 0.05 M $CsPF_6$ additive.

anodes after 100 charge/discharge cycles. The Li electrode in the cell without additive (see Figure 4a) exhibits clear dendritic growth behavior, but no dendritic Li was observed in the cell with additives (see Figure 4b). These cells demonstrated excellent long-term cycling stability (only 4% capacity fade in 660 cycles when charged/discharged at 1 C rate) as shown in Figure 5. Charge/discharge voltage profiles of the cell are shown in Figure S5 in the Supporting Information.

It should be noted that the main purpose of the above long-term cycling test is to prove the absence of battery short associated with Li dendrite growth, which is always encountered during cycling of conventional Li metal batteries when a conventional electrolyte is used. The high Coulombic efficiency (99.86%) shown in Figure 5 is associated with Li|$Li_4Ti_5O_{12}$ cell, which contain excess amount of Li metal anode. To further evaluate the Columbic efficiency of Li deposition, a method proposed by Aurbach et al.[39] has been used (see section 2.2 in the Supporting Information for the details of the measurement). The average Coulombic efficiency of Li deposition was found to be 76.5% in 1.0 M $LiPF_6$/PC

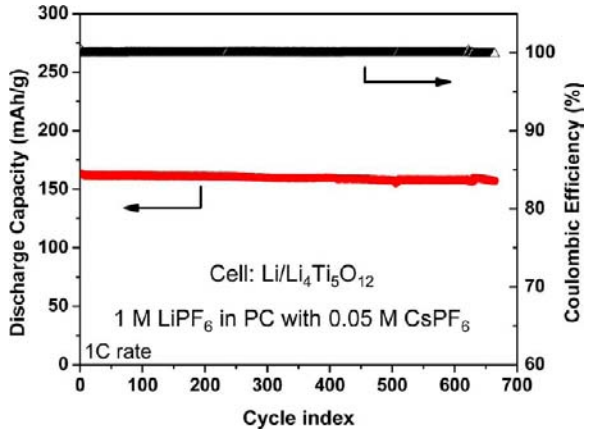

Figure 5. Long-term cycling stability and Coulombic efficiency of Li|$Li_4Ti_5O_{12}$ cell containing electrolyte of 1 M $LiPF_6$/PC with 0.05 M $CsPF_6$ additive.

electrolyte and 76.6% in the electrolyte with addition of 0.05 M $CsPF_6$. The low Coulombic efficiency of Li deposition in PC-based electrolytes is mainly due to the poor SEI layer formed on Li metal surface from the decomposition of PC solvent, which cannot prevent further reactions between Li metal and electrolyte components. We also investigated the deposition of Li film in several other conventional electrolyte solvents. It is found that cyclic carbonate solvents (ethylene carbonate, PC, vinylene carbonate, vinyl ethylene carbonate, fluoroethylene carbonate) lead to smoother and more uniform lithium deposition than do linear carbonate solvents (dimethyl carbonate, ethyl methyl carbonate). To utilize lithium metal as an anode in practical rechargeable Li metal batteries, a good combination of electrolyte solvent, salt, and additives still needs to be identified so both high Coulombic efficiency and dendrite-free morphology of Li deposition can be realized.

Simulation of Li Deposition Based on SHES Mechanism. To further investigate the proposed SHES mechanism, computational modeling was conducted to simulate Li deposition from the electrolyte containing 1 M $LiPF_6$ in PC as the main salt and 0.05 M $CsPF_6$ as the additive as described in the Experimental Section. The simulations reveal a sharp increase in the electrostatic potential at the Li deposition site (see Figure S4a in the Supporting Information). This leads to redistribution of cations and anions in the electrolyte solution and at the electrode surface. Li^+ and Cs^+ accumulate in the high potential region around a protrusion on the Li metal electrode. Li^+ comes in close vicinity to the protrusion and deposits, while Cs^+ adsorbs in areas of high opposite charge on the electrode surface, forming a diffuse double layer and partially screening the electrostatic potential of the protrusion. This effect is a direct consequence of stronger electrostatic correlation, or dispersion, interactions between Cs^+ ions. Strong dispersion interactions between Cs^+ ions induce preferential accumulation of Cs^+ at the sites with higher potentials and lead to the formation of a dense screening layer.

Simulations were repeated for 24 steps. The initial Cs^+ to Li^+ ratio is 1:17 at the surface as opposed to 1:20 in the bulk (see Figure S4b in the Supporting Information). Because Li deposition decreases its local effective concentration, this ratio decreases with the growth of the protrusion until it reaches 1:14, at which point dendrite growth at this site stops due to strong electrostatic screening of the site by Cs^+. Moreover, Cs^+-induced shielding of Li^+ from the protrusion

dx.doi.org/10.1021/ja312241y | J. Am. Chem. Soc. 2013, 135, 4450−4456

leads to preferential Li deposition adjacent to the protuberance rather than at the tip, even during initial stages of Li deposition. This results in the growth of islands on the electrode surface in the presence of Cs^+ rather than needle-like dendrites, which are energetically favorable in the control electrolyte.

When lithium was deposited in an electrolyte containing 1 M $LiPF_6$ in PC, dendrite growth starts as a narrow pyramid and becomes a two-atom wide column after 24 deposition steps (see movie S3 in the Supporting Information). Li deposition on top of the protrusion is driven by its high electric potential, which induces Li^+ accumulation at the tip of the protrusion. In contrast, when lithium was deposited in an electrolyte containing 1 M $LiPF_6$ and 0.05 M $CsPF_6$ additive in PC, weaker electrostatic correlation repulsion between Cs^+ ions as compared to that between Li^+ ions leads to preferential accumulation of Cs^+ in the vicinity of the protrusions causing the electrostatic screening of the high-potential site. Therefore, Li is deposited adjacent to the protrusion, rather than on top of it. This results in a lateral layer-by-layer growth after 24 deposition steps (see movie S4 in the Supporting Information). Snapshots of the simulated Li deposition process without, and with, Cs^+ additive after 24 deposition steps are shown in Figure 6a and b, respectively. The protrusion grown in the presence of Cs^+ has a blunted, dome shape, while in the control electrolyte, needle-like dendrite growth is observed.

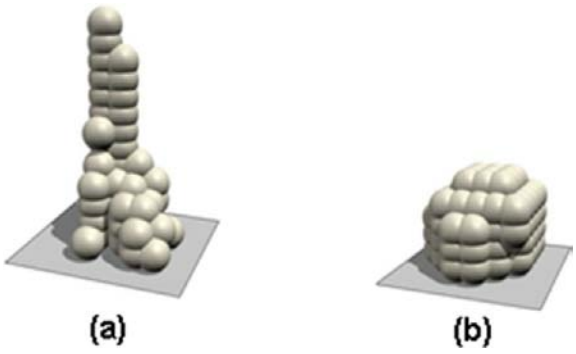

Figure 6. Simulated Li deposition onto a flat electrode surface from (a) 1 M $LiPF_6$ solution in PC and (b) from 1 M $LiPF_6$ + 0.05 M $CsPF_6$ solution in PC.

CONCLUDING REMARKS

We have demonstrated that the SHES mechanism fundamentally changes the morphology of the deposited Li from needle-like dendrites to mirror-like films, or films that consist of merged, fine spherical particles. Further, these additives are not consumed during Li deposition and remain effective after long-term cycling of the batteries. The proposed SHES mechanism is fundamentally different from previous approaches used to suppress dendritic growth based on (i) mechanical suppression or (ii) additives that are consumed during cycling, but do not eliminate the self-amplification growth behavior of the dendrites. This method is not only effective in preventing dendrite growth in Li metal batteries, but preliminary results on Li-ion cells show promise in suppression of metal plating at high overcharge. This approach may also prevent dendritic growth in other rechargeable metal batteries (such as Na-ion, Mg-ion, Zn-air, etc.) and have transformational impact on the surface quality of films derived from many electrodeposition processes. Furthermore, the fundamental scientific principles that transform a chaotic/dendritic growth pattern to an ordered/spheroidal growth pattern may also explain other naturally occurring phenomena and provide possible guidelines to control heterogeneous nucleation and growth in other fields.

At last, we need to indicate that, although the SHES mechanism has addressed the dendritic morphology problem encountered during Li deposition, Coulombic efficiency of Li deposition in the electrolytes used in this work is still relatively low. A good combination of electrolyte solvent, salt, and additives still needs to be identified to obtain both dendrite-free morphology and high Coulombic efficiency of metal deposition at the same time, which is required for long-term cycling operation of lithium and other metal anode in electrochemical devices.

ASSOCIATED CONTENT

Supporting Information

XPS spectra, EDX analysis, in situ optical observation of the deposited lithium film; simulation of the electrostatic potential and ion concentrations; and supplementary methods and movies. This material is available free of charge via the Internet at http://pubs.acs.org.

AUTHOR INFORMATION

Corresponding Author

jiguang.zhang@pnnl.gov; wu.xu@pnnl.gov

Notes

The authors declare no competing financial interest.

ACKNOWLEDGMENTS

We thank Mr. Honghao Chen, Dr. Jianming Zheng, and Dr. Eduard Nasybulin of Pacific Northwest National Laboratory (PNNL) for assistance in the experimental work of substrate preparation; Dr. Jarrod Crum of PNNL for help with the SEM measurement; and Prof. Chunlin Zhou and Prof. Haojie Liu of Tianjin Institute of Power Sources for help with material preparation. This work was supported by the Assistant Secretary for Energy Efficiency and Renewable Energy, Office of Vehicle Technology of the U.S. Department of Energy (DOE), and the Laboratory Directed Research and Development fund of PNNL. The XPS work was performed at the Environmental Molecular Sciences Laboratory, a national scientific user facility sponsored by the DOE's Office of Biological and Environmental Research and located at PNNL. The modeling work is supported by the DOE Office of Basic Energy Sciences, Division of Materials Sciences and Engineering.

REFERENCES

(1) Goodenough, J. B.; Abruña, H. D.; Buchanan, M. V. *Report of the Basic Energy Sciences Workshop on Electrical Energy Storage*, April 2–4, 2007; http://web.anl.gov/energy-storage-science/publications/EES_rpt.pdf.

(2) Whittingham, M. S. *Proc. IEEE* **2012**, *100*, 1518–1534.

(3) Whittingham, M. S.; https://www.ornl.gov/ccsd_registrations/battery/presentations/Session1-820-Whittingham.pdf.

(4) Vincent, C. A. *Solid State Ionics* **2000**, *134*, 159–167.

(5) Aurbach, D.; Cohen, Y. *J. Electrochem. Soc.* **1996**, *143*, 3525–3532.

(6) Bruce, P. G.; Freunberger, S. A.; Hardwick, L. J.; Tarascon, J.-M. *Nat. Mater.* **2012**, *11*, 19–29.

(7) Ji, X. L.; Lee, K. T.; Nazar, L. F. *Nat. Mater.* **2009**, *8*, 500–506.

(8) Girishkumar, G.; McCloskey, B.; Luntz, A. C.; Swanson, S.; Wilcke, W. *J. Phys. Chem. Lett.* **2010**, *1*, 2193–2203.

(9) Lee, J.-S.; Kim, S. T.; Cao, R.; Choi, N.-S.; Liu, M.; Lee, K. T.; Cho, J. *Adv. Energy Mater.* **2011**, *1*, 34−50.
(10) Chianelli, R. R. *J. Cryst. Growth* **1976**, *34*, 239−244.
(11) Aurbach, D.; Zinigrad, E.; Cohen, Y.; Teller, H. *Solid State Ionics* **2002**, *148*, 405−416.
(12) Gireaud, L.; Grugeon, S.; Laruelle, S.; Yrieix, B.; Tarascon, J.-M. *Electrochem. Commun.* **2006**, *8*, 1639−1649.
(13) Brissot, C.; Rosso, M.; Chazalviel, J.-N.; Lascaud, S. *J. Power Sources* **1999**, *81*−*82*, 925−929.
(14) Chandrashekar, S.; Trease, N. M.; Chang, H. J.; Du, L.-S.; Grey, C. P.; Jerschow, A. *Nat. Mater.* **2012**, *11*, 311−315.
(15) Kominato, A.; Yasukawa, E.; Sato, N.; Ijuuin, T.; Tsahina, H.; Mori, S. *J. Power Sources* **1997**, *68*, 471−475.
(16) Aurbach, D.; Weissman, I.; Zaban, A.; Chusid, O. *Electrochim. Acta* **1994**, *39*, 51−71.
(17) Odziemkowski, M.; Krell, M.; Irish, D. E. *J. Electrochem. Soc.* **1992**, *139*, 3052−3063.
(18) Monroe, C.; Newman, J. *J. Electrochem. Soc.* **2005**, *152*, A396−A404.
(19) Tang, M.; Albertus, P.; Newman, J. *J. Electrochem. Soc.* **2009**, *156*, A390−A399.
(20) Yamaki, J.-I.; Tobishima, S.-I.; Hayashi, K.; Saito, K.; Nemoto, Y.; Arakawa, M. *J. Power Sources* **1998**, *74*, 219−227.
(21) Ota, H.; Shima, K.; Ue, M.; Yamaki, J.-I. *Electrochim. Acta* **2004**, *49*, 565−572.
(22) Naoi, K.; Mori, M.; Naruoka, Y.; Lamanna, W. M.; Atanasoski, R. *J. Electrochem. Soc.* **1999**, *146*, 462−469.
(23) Shiraishi, S.; Kanamura, K.; Takehara, Z.-I. *J. Electrochem. Soc.* **1999**, *146*, 1633−1639.
(24) Ota, H.; Wang, X. M.; Yasukawa, E. *J. Electrochem. Soc.* **2004**, *151*, A427−A436.
(25) Kanamura, K.; Tamura, H.; Shiraishi, S.; Takeha, Z.-I. *J. Electroanal. Chem.* **1995**, *394*, 49−62.
(26) Mogi, R.; Inaba, M.; Jeong, S.-K.; Iriyama, Y.; Abe, T.; Ogumi, Z. *J. Electrochem. Soc.* **2002**, *149*, A1578−A1583.
(27) Lee, Y. M.; Seo, J. E.; Lee, Y.-G.; Lee, S. H.; Cho, K. Y.; Park, J.-K. *Electrochem. Solid-State Lett.* **2007**, *10*, A216−A219.
(28) Yoon, S.; Lee, J.; Kim, S.-O.; Sohn, H.-J. *Electrochim. Acta* **2008**, *53*, 2501−2506.
(29) Zhamu, A.; Chen, G.; Liu, C.; Neff, D.; Fang, Q.; Yu, Z.; Xiong, W.; Wang, Y.; Wang, X.; Jang, B. Z. *Energy Environ. Sci* **2012**, *5*, 5701−5707.
(30) Matsuda, Y.; Morita, M.; Nigo, H. In *Primary and Secondary Lithium Batteries*; Abraham, K. M., Salomon, M., Eds.; The Electrochemical Society Proceedings Series: Pennington, NJ, 1991; PV 91−3, p 272.
(31) Matsuda, Y. *J. Power Sources* **1993**, *43*−*44*, 1−7.
(32) Ishikawa, M.; Yoshitake, S.; Morita, M.; Matsuda, Y. *J. Electrochem. Soc.* **1994**, *141*, L159−L161.
(33) Ishikawa, M.; Morita, M.; Matsuda, Y. *J. Power Sources* **1997**, *68*, 501−505.
(34) Balsara, N. P.; Singh, M.; Eitouni, H. B.; Gomez, E. D. U.S. Patent Appl. No. 2009/0263725 A1.
(35) Visco, S. J.; Nimon, E.; Katz, B.; Jonghe, L. C. D.; Chu, M.-Y. *Proceedings of the 12th International Meeting on Lithium Batteries*; The Electrochemical Society: Nara, Japan, June 27−July 2, 2004; Abstract No. 396.
(36) Stark, J. K.; Ding, Y.; Kohl, P. A. *J. Electrochem. Soc.* **2011**, *158*, A1100−A1105.
(37) Sushko, M. L.; Liu, J. *J. Phys. Chem. B* **2010**, *114*, 3847−3854.
(38) Wu, J. Z.; Li, Z. D. *Annu. Rev. Phys. Chem.* **2007**, *58*, 85−112.
(39) Aurbach, D.; Markovsky, B.; Levi, M. D.; Levi, E.; Schechter, A.; Moshkovich, M.; Cohen, Y. *J. Power Sources* **1999**, *81*−*82*, 95−111.